zumab resulted in morphologic stabilization of the PCV lesions, but not in visual recovery.[34] The reason for the poor change in VA seen in the PDT group after the combined therapy is unclear, although damage of the choriocapillaris or retinal pigment epithelium resulting from previous PDT may be involved. Rather, recent reports have shown the association of some genetic factors to the response to PDT and to subsequent visual prognosis in eyes with PCV.[43,44] Originally, the PDT group may consist of the eyes that have genetically poor VA prognosis.

To date, limited information is available on combined therapy for PCV that is refractory to anti-VEGF therapy. The current study has shown that some visual recovery can be expected when PDT is combined with ranibizumab, even in eyes with PCV that previously were treated with anti-VEGF agents. Because the effect of anti-VEGF therapy on polypoidal lesions is limited,[13–18,21–24] combined therapy may well be a treatment option when recurrent or persistent exudative change is seen after anti-VEGF treatments.

For treatment of PCV, one of the most vision-threatening complications of PDT is extensive postoperative hemorrhage.[45,46] In a previous article on PCV treated with PDT, Hirami and associates reported that postoperative subretinal hemorrhage was seen in 28 (30.8%) of 91 eyes, and that bleeding resulted in a vitreous hemorrhage in 6 eyes.[45] Recent reports by Gomi and associates and by Sato and associates suggested a lower incidence of subretinal hemorrhage when the PDT was combined with bevacizumab.[35,36] In the current study, 2 eyes in the treatment-naïve group had an extensive subretinal hemorrhage (larger than 4 disc areas) after such combined therapy, although the hemorrhage was absorbed spontaneously with no decrease in VA. In addition, 3 eyes in the PDT group had an extensive subretinal hemorrhage after treatment, and this resulted in vitreous hemorrhage in 2 eyes, so it is uncertain whether combined therapy actually reduces the posttreatment hemorrhagic complications. However, similar to PDT alone, even if PDT is combined with anti-VEGF agents, physicians need to keep in mind the risk to their patients of these complications.

Major limitations of the current study are its retrospective nature, its small sample size, and its lack of control individuals. Furthermore, we used a Landolt chart, which is based on an uneven spatial gradient scale, for the measurement of VA. However, despite these shortcomings, our findings suggest that PDT combined with intravitreal injections of ranibizumab results in rapid regression of the polypoidal lesions and exudative changes and often results in improvement of VA in eyes with treatment-naïve PCV. Patients with PCV treated with PDT combined with ranibizumab do have a risk of posttreatment hemorrhagic complications. However, because our findings are based on an observation period of only 12 months, it remains unclear whether PDT in combination with ranibizumab reduces the recurrence rate of PCV. Because the long-term efficacy of PDT alone is not as promising as was thought initially, prospective long-term studies are needed to determine the efficacy and safety of combined therapy for PCV.

PUBLICATION OF THIS ARTICLE WAS SUPPORTED IN PART BY GRANT-IN-AID FOR SCIENTIFIC RESEARCH 21592256 FROM THE Japan Society for the Promotion of Science (JSPS), Tokyo, Japan; and the Japan National Society for the Prevention of Blindness, Tokyo, Japan. The authors indicate no financial conflict of interest. Involved in Conception and design of the study (K.T., A.T., K.Y., S.O., N.Y.); Data collection (K.T., H.T., O.A., Y.N.); Analysis and interpretation of data (K.T.,. A.T., K.Y., S.O., H.T., O.A., Y.N., N.Y.); Writing of the article (K.T., A.T.); Critical revision of the article (K.Y., S.O., H.T., O.A., Y.N., N.Y.); and Final approval of the article (K.T., A.T., K.Y., S.O., H.T., O.A., Y.N., N.Y.). This study was approved by the Institutional Review Board at Kyoto University Graduate School of Medicine and adhered to the tenets of the Declaration of Helsinki. For treatment, written informed consent was obtained from each patient. According to the guidelines, it is not mandatory to obtain informed consent from the patients for a retrospective study in which the researchers review only medical records.

REFERENCES

1. Rosenfeld PJ, Brown DM, Heier JS, et al. Ranibizumab for neovascular age-related macular degeneration. N Engl J Med 2006;355(14):1419–1431.
2. Brown DM, Kaiser PK, Michels M, et al. Ranibizumab versus verteporfin for neovascular age-related macular degeneration. N Engl J Med 2006;355(14):1432–1444.
3. Yannuzzi LA, Wong DW, Sforzolini BS, et al. Polypoidal choroidal vasculopathy and neovascularized age-related macular degeneration. Arch Ophthalmol 1999;117(11):1503–1510.
4. Yannuzzi LA, Ciardella A, Spaide RF, Rabb M, Freund KB, Orlock DA. The expanding clinical spectrum of idiopathic polypoidal choroidal vasculopathy. Arch Ophthalmol 1997;115(4):478–485.
5. Uyama M, Matsubara T, Fukushima I, et al. Idiopathic polypoidal choroidal vasculopathy in Japanese patients. Arch Ophthalmol 1999;117(8):1035–1042.
6. Kleiner RC, Brucker AJ, Johnston RL. The posterior uveal bleeding syndrome. Retina 1990;10(1):9–17.
7. Stern RM, Zakov ZN, Zegarra H, Gutman FA. Multiple recurrent serosanguineous retinal pigment epithelial detachments in black women. Am J Ophthalmol 1985;100(4):560–569.
8. Yannuzzi LA, Sorenson J, Spaide RF, Lipson B. Idiopathic polypoidal choroidal vasculopathy (IPCV). Retina 1990;10(1):1–8.
9. Spaide RF, Yannuzzi LA, Slakter JS, Sorenson J, Orlach DA. Indocyanine green videoangiography of idiopathic polypoidal choroidal vasculopathy. Retina 1995;15(2):100–110.
10. Wells JA, Murthy R, Chibber R, et al. Levels of vascular endothelial growth factor are elevated in the vitreous of

patients with subretinal neovascularisation. Br J Ophthalmol 1996;80(4):363–366.
11. Tong JP, Chan WM, Liu DT, et al. Aqueous humor levels of vascular endothelial growth factor and pigment epithelium-derived factor in polypoidal choroidal vasculopathy and choroidal neovascularization. Am J Ophthalmol 2006; 141(3):456–462.
12. Matsuoka M, Ogata N, Otsuji T, Nishimura T, Takahashi K, Matsumura M. Expression of pigment epithelium derived factor and vascular endothelial growth factor in choroidal neovascular membranes and polypoidal choroidal vasculopathy. Br J Ophthalmol 2004;88(6):809–815.
13. Ghajarnia M, Kurup S, Eller A. The therapeutic effects of intravitreal bevacizumab in a patient with recalcitrant idiopathic polypoidal choroidal vasculopathy. Semin Ophthalmol 2007;22(2):127–131.
14. Lai TY, Chan WM, Liu DT, Luk FO, Lam DS. Intravitreal bevacizumab (Avastin) with or without photodynamic therapy for the treatment of polypoidal choroidal vasculopathy. Br J Ophthalmol 2008;92(5):661–666.
15. Gomi F, Sawa M, Sakaguchi H, et al. Efficacy of intravitreal bevacizumab for polypoidal choroidal vasculopathy. Br J Ophthalmol 2008;92(1):70–73.
16. Song JH, Byeon SH, Lee SC, Koh HJ, Kwon OW. Short-term safety and efficacy of a single intravitreal bevacizumab injection for the management of polypoidal choroidal vasculopathy. Ophthalmologica 2009;223(2):85–92.
17. Pai SA, Shetty R. Sequential therapy with intravitreal bevacizumab and photodynamic therapy for idiopathic polypoidal choroidal vasculopathy. Acta Ophthalmol 2009; 87(7):806–807.
18. Lee SY, Kim JG, Joe SG, Chung H, Yoon YH. The therapeutic effects of bevacizumab in patients with polypoidal choroidal vasculopathy. Korean J Ophthalmol 2008; 22(2):92–99.
19. Cho M, Barbazetto IA, Freund KB. Refractory neovascular age-related macular degeneration secondary to polypoidal choroidal vasculopathy. Am J Ophthalmol 2009;148(1): 70–78.
20. Stangos AN, Gandhi JS, Nair-Sahni J, Heimann H, Pournaras CJ, Harding SP. Polypoidal choroidal vasculopathy masquerading as neovascular age-related macular degeneration refractory to ranibizumab. Am J Ophthalmol 2010; 150(5):666–673.
21. Tsujikawa A, Ooto S, Yamashiro K, Tamura H, Otani A, Yoshimura N. Treatment of polypoidal choroidal vasculopathy by intravitreal injection of bevacizumab. Jpn J Ophthalmol 2010;54(4):310–319.
22. Kokame GT, Yeung L, Lai JC. Continuous anti-VEGF treatment with ranibizumab for polypoidal choroidal vasculopathy: 6-month results. Br J Ophthalmol 2010;94(3):297–301.
23. Rouvas AA, Papakostas TD, Ntouraki A, Douvali M, Vergados I, Ladas ID. Photodynamic therapy, ranibizumab, and ranibizumab with photodynamic therapy for the treatment of polypoidal choroidal vasculopathy. Retina 2011;31(3):464–474.
24. Cheng CK, Peng CH, Chang CK, Hu CC, Chen LJ. One-year outcomes of intravitreal bevacizumab (Avastin) therapy for polypoidal choroidal vasculopathy. Retina 2011; 31(5):846–856.
25. Hikichi T, Ohtsuka H, Higuchi M, et al. Improvement of angiographic findings of polypoidal choroidal vasculopathy after intravitreal injection of ranibizumab monthly for 3 months. Am J Ophthalmol 2010;150(5):674–682.
26. Spaide RF, Donsoff I, Lam DL, et al. Treatment of polypoidal choroidal vasculopathy with photodynamic therapy. Retina 2002;22(5):529–535.
27. Chan WM, Lam DS, Lai TY, et al. Photodynamic therapy with verteporfin for symptomatic polypoidal choroidal vasculopathy: one-year results of a prospective case series. Ophthalmology 2004;111(8):1576–1584.
28. Otani A, Sasahara M, Yodoi Y, et al. Indocyanine green angiography: guided photodynamic therapy for polypoidal choroidal vasculopathy. Am J Ophthalmol 2007;144(1): 7–14.
29. Gomi F, Ohji M, Sayanagi K, et al. One-year outcomes of photodynamic therapy in age-related macular degeneration and polypoidal choroidal vasculopathy in Japanese patients. Ophthalmology 2008;115(1):141–146.
30. Silva RM, Figueira J, Cachulo ML, Duarte L, Faria de Abreu JR, Cunha-Vaz JG. Polypoidal choroidal vasculopathy and photodynamic therapy with verteporfin. Graefes Arch Clin Exp Ophthalmol 2005;243(10):973–979.
31. Kurashige Y, Otani A, Sasahara M, et al. Two-year results of photodynamic therapy for polypoidal choroidal vasculopathy. Am J Ophthalmol 2008;146(4):513–519.
32. Tsuchiya D, Yamamoto T, Kawasaki R, Yamashita H. Two-year visual outcomes after photodynamic therapy in age-related macular degeneration patients with or without polypoidal choroidal vasculopathy lesions. Retina 2009; 29(7):960–965.
33. Akaza E, Mori R, Yuzawa M. Long-term results of photodynamic therapy of polypoidal choroidal vasculopathy. Retina 2008;28(5):717–722.
34. Romano MR, Cipollone U, Semeraro F, Rinaldi M, Costagliola C. Combined photodynamic therapy and intravitreal bevacizumab for idiopathic polypoidal choroidal vasculopathy: one-year follow-up. Clin Ophthalmol 2010;4:1237–1241.
35. Sato T, Kishi S, Matsumoto H, Mukai R. Combined photodynamic therapy with verteporfin and intravitreal bevacizumab for polypoidal choroidal vasculopathy. Am J Ophthalmol 2010;149(6):947–954.
36. Gomi F, Sawa M, Wakabayashi T, Sasamoto Y, Suzuki M, Tsujikawa M. Efficacy of intravitreal bevacizumab combined with photodynamic therapy for polypoidal choroidal vasculopathy. Am J Ophthalmol 2010;150(1):48–54.
37. Zuo C, Wen F, Li J, Liu Y, Li M. Transitions of multifocal electroretinography following combined intravitreal bevacizumab and photodynamic therapy for polypoidal choroidal vasculopathy. Doc Ophthalmol 2009;119(1):29–36.
38. Moon SW, Kim MS, Kim ES, Yu SY, Kwak HW. Photodynamic therapy combined with intravitreal injection of vascular endothelial growth factor antibody for polypoidal choroidal vasculopathy. Ophthalmologica 2011;225(3):169–175.
39. Ruamviboonsuk P, Tadarati M, Vanichvaranont S, Hanutsaha P, Pokawattana N. Photodynamic therapy combined with ranibizumab for polypoidal choroidal vasculopathy: results of a 1-year preliminary study. Br J Ophthalmol 2010;94(8):1045–1051.
40. Guidelines for using verteporfin (Visudyne) in photodynamic therapy for choroidal neovascularization due to age-

related macular degeneration and other causes: update. Retina 2005;25(2):119–134.
41. Yamashiro K, Tsujikawa A, Nishida A, Mandai M, Kurimoto Y. Recurrence of polypoidal choroidal vasculopathy after photodynamic therapy. Jpn J Ophthalmol 2008;52(6):457–462.
42. Schmidt-Erfurth U, Schlötzer-Schrehard U, Cursiefen C, Michels S, Beckendorf A, Naumann GO. Influence of photodynamic therapy on expression of vascular endothelial growth factor (VEGF), VEGF receptor 3, and pigment epithelium-derived factor. Invest Ophthalmol Vis Sci 2003; 44(10):4473–4480.
43. Sakurada Y, Kubota T, Imasawa M, Mabuchi F, Tanabe N, Iijima H. Association of LOC387715 A69S genotype with visual prognosis after photodynamic therapy for polypoidal choroidal vasculopathy. Retina 2010;30(10):1616–1621.
44. Nakata I, Yamashiro K, Yamada R, et al. Genetic variants in pigment epithelium-derived factor influence response of polypoidal choroidal vasculopathy to photodynamic therapy. Ophthalmology 2011;118(7):1408–1415.
45. Hirami Y, Tsujikawa A, Otani A, et al. Hemorrhagic complications after photodynamic therapy for polypoidal choroidal vasculopathy. Retina 2007;27(3):335–341.
46. Ojima Y, Tsujikawa A, Otani A, Hirami Y, Aikawa H, Yoshimura N. Recurrent bleeding after photodynamic therapy in polypoidal choroidal vasculopathy. Am J Ophthalmol 2006;141(5):958–960.

REPORTING VISUAL ACUITIES

The AJO encourages authors to report the visual acuity in the manuscript using the same nomenclature that was used in gathering the data provided they were recorded in one of the methods listed here. This table of equivalent visual acuities is provided to the readers as an aid to interpret visual acuity findings in familiar units.

Table of Equivalent Visual Acuity Measurements

Snellen Visual Acuities				
4 Meters	6 Meters	20 Feet	Decimal Fraction	LogMAR
4/40	6/60	20/200	0.10	+1.0
4/32	6/48	20/160	0.125	+0.9
4/25	6/38	20/125	0.16	+0.8
4/20	6/30	20/100	0.20	+0.7
4/16	6/24	20/80	0.25	+0.6
4/12.6	6/20	20/63	0.32	+0.5
4/10	6/15	20/50	0.40	+0.4
4/8	6/12	20/40	0.50	+0.3
4/6.3	6/10	20/32	0.63	+0.2
4/5	6/7.5	20/25	0.80	+0.1
4/4	6/6	20/20	1.00	0.0
4/3.2	6/5	20/16	1.25	−0.1
4/2.5	6/3.75	20/12.5	1.60	−0.2
4/2	6/3	20/10	2.00	−0.3

From Ferris FL III, Kassoff A, Bresnick GH, Bailey I. New visual acuity charts for clinical research. Am J Ophthalmol 1982;94:91–96.

Biosketch

Kaoruko Tomita, MD, is a graduate of the Graduate School of Medicine of Osaka City University. She completed an ophthalmology residency at Kobe City General Hospital and a fellowship at the Osaka City University Hospital in Japan. Following the fellowship, she worked at Osaka City General Hospital, and currently works at Nakano Eye Clinic. She continues researching macular diseases at Kyoto University Graduate School of Medicine, Kyoto, Japan.

Jpn J Ophthalmol (2011) 55:435–443
DOI 10.1007/s10384-011-0061-z

CLINICAL INVESTIGATION

VEGF gene polymorphism and response to intravitreal bevacizumab and triple therapy in age-related macular degeneration

Isao Nakata · Kenji Yamashiro · Hideo Nakanishi · Akitaka Tsujikawa · Atsushi Otani · Nagahisa Yoshimura

Received: 23 May 2010 / Accepted: 19 April 2011 / Published online: 9 July 2011

Abstract
Purpose To investigate the association between the vascular endothelial growth factor (VEGF) gene and response to either intravitreal bevacizumab (IVB) or photodynamic therapy with intravitreal triamcinolone acetonide and IVB (triple therapy) for neovascular age-related macular degeneration (AMD).
Methods The study consisted of 94 patients with neovascular AMD who underwent IVB and 79 patients with neovascular AMD who underwent triple therapy. Genotypes were determined for four selected tagging single-nucleotide polymorphism (SNP)s of the VEGF gene.
Results Of the four SNPs studied, one SNP (rs699946) was associated significantly with visual acuity (VA) changes 12 months after treatment—irrespective of whether they received IVB alone ($P = 0.044$) or triple therapy 0.010). Baseline VA was not significantly different among the three genotypes of rs699946 in either treatment group. There were no significant differences in the number of treatments, incidence of recurrence, or the period until the recurrence according to VEGF rs699946 genetic variant.
Conclusions The VEGF gene SNP rs699946 was associated with response to IVB alone and to triple therapy in this study. The G allele in SNP rs699946 can thus be applied as a marker for better visual prognosis in patients with neovascular AMD who receive either IVB or triple therapy.

Keywords Bevacizumab · Photodynamic therapy · Vascular endothelial growth factor

I. Nakata · K. Yamashiro (✉) · H. Nakanishi · A. Tsujikawa · A. Otani · N. Yoshimura
Department of Ophthalmology and Visual Sciences, Kyoto University Graduate School of Medicine, 54 Kawahara, Shogoin, Sakyo, Kyoto 606-8507, Japan
e-mail: yamashro@kuhp.kyoto-u.ac.jp

I. Nakata · H. Nakanishi
Center for Genomic Medicine, Kyoto University Graduate School of Medicine, Kyoto, Japan

Introduction

Age-related macular degeneration (AMD) is the leading cause of severe impairment of the visual function in people 50 years of age or older who reside in industrialized countries [1]. Recent treatment for neovascular AMD includes photodynamic therapy (PDT) [2] and anti-vascular endothelial growth factor (VEGF) therapy [3–8]. Because VEGF is expressed in choroidal neovascularization (CNV) [9–11] and induces an exudative change in the retina, anti-VEGF drugs can inactivate CNV and reduce the retinal exudative change. In addition to their direct role as a treatment for AMD, anti-VEGF drugs have been used in combination with PDT to suppress the VEGF upregulation that is typically induced by PDT. Recently, triple therapy using PDT combined with intravitreal bevacizumab (IVB) and intravitreal triamcinolone acetonide (IVTA) was introduced [12, 13].

VEGF is a major molecular mediator of neovascularization and of vascular permeability [14], and its expression is upregulated under hypoxic conditions. The VEGF gene is located on chromosome 6p12, and the coding region spans approximately 16.3 kb. Polymorphisms of the VEGF gene have been shown to be associated with levels of VEGF in both serum [15–17] and vitreous [18]. VEGF polymorphisms are associated with the prognosis of several diseases associated with VEGF [19–24]. Recently, Immonen et al. [25] demonstrated that VEGF

gene polymorphisms affect the anatomic outcome of AMD after PDT. However, the association of VEGF gene polymorphism with the visual prognosis of patients with AMD has not been examined and, despite the anatomic success after PDT, fibrosis can attenuate the relatively good visual outcomes, just as residual lesions of serous detachment after PDT do not always result in lower visual acuity (VA). It would thus be important to know exactly what factor(s) may determine the visual prognosis of eyes with AMD that have undergone treatment.

Because IVB treatment and triple therapy include anti-VEGF drugs, it is conceivable that VEGF gene polymorphism correlates with the results of this AMD treatment. In this study we sought to determine if there is any association between VEGF genotype and the response of neovascular AMD to IVB or to triple therapy.

Materials and methods

Patients and methods

This study was performed in accordance with the tenets of the Declaration of Helsinki and approved by the Institutional Review Board/Ethics Committee of Kyoto University Graduate School of Medicine, Kyoto, Japan. All patients provided written informed consent after the risks and benefits of the treatment were fully explained to them. For this retrospective study, we reviewed the medical records of 173 patients with neovascular AMD who had either received IVB alone (IVB group) or PDT combined with IVB and IVTA (triple-therapy group) at Kyoto University Hospital between May 2006 and November 2008. All patients included in the study had subfoveal CNV associated with AMD, VA better than 1.0, as the logarithm of the minimum angle of resolution (logMAR) at baseline, and were 50 years of age or older; patients were excluded if they had undergone surgical treatment for their AMD before either the IVB or triple therapy.

Before treatment, each patient had undergone a comprehensive ophthalmologic examination, including measurement of best-corrected VA, intraocular pressure testing, indirect ophthalmoscopy, and slitlamp biomicroscopy with a contact lens. Best-corrected VA was measured with a Landolt chart and converted to a logMAR. After fundus photographs were taken, fluorescein and indocyanine green angiography were performed and the retinal cross section was examined with optical coherence tomography (OCT). Diagnosis of polypoidal choroidal vasculopathy (PCV) was based on indocyanine green angiography, which showed a branching vascular network terminating in polypoidal swelling.

The IVB group had an intravitreal injection of 1.25 mg bevacizumab one to three times as the initial treatment. The second and/or third injections were performed at 1-month intervals, when angiography and/or OCT examination showed remnant macular exudative changes (serous retinal detachment or retinal edema on OCTs or angiographic leakage seen on FAs). For the patients in the triple-therapy group, 1.25 mg bevacizumab and 2 mg TA were administered intravitreally 3 to 4 days before the PDT. The treatment decisions were made by retina specialists at the Department of Ophthalmology at Kyoto University Hospital, who were unaware of the genotype of the patients. Retreatment was performed when an eye showed severe leakage of fluorescein dye during the late phase of fluorescein angiography or serous retinal detachment because of residual active CNV as seen on OCT usually after a 3-month interval. In the IVB group, an intravitreal anti-VEGF drug was given when recurrence was noted. During the sequence of monthly injections for initial treatment, we did not encounter any recurrence of exudative changes. In the triple-therapy group, PDT either with or without an intravitreal anti-VEGF drug or anti-VEGF treatment was performed for any recurrence that occurred.

Single nucleotide polymorphism selection and Genotyping

Four tagging VEGF single-nucleotide polymorphism (SNP)s were selected for investigation—two SNPs on the promoter region, rs699946 and rs699947, and two intronic SNPs, rs3025033 and 3025035. The four tagging VEGF SNPs provided 100% coverage for all common (minor allele frequency of more than 20%) HapMap [26] SNPs within a 26.3 kilobase region (16.3-kb gene length; 10 kb upstream) spanning the VEGF gene on chromosome 6 (r^2 threshold of 0.95). Genomic DNAs were prepared from peripheral blood using a DNA extraction kit (QuickGene-610L; Fujifilm, Minato, Tokyo, Japan). Genotyping was performed using the Taqman SNP assay with the ABI Prism 7700 system (Applied Biosystems, Foster City, CA, USA).

Data analysis

Descriptive statistics for all demographic and clinical variables were calculated and comparisons made using the unpaired t test for means with continuous data (e.g., age) and the chi-squared test for categorical data (e.g., gender). Visual acuity before and after treatment were compared among genotypes by use of analysis of variance (ANOVA) test and VA changes among genotypes were evaluated by use of the Jonckheere–Terpstra trend test, which is a

nonparametric test for ordered differences among classes [27]. Significance was defined at the 5% level.

Results

Patients with neovascular AMD who underwent treatment with IVB alone ($n = 94$) or with triple therapy ($n = 79$) were enrolled in this study. Demographic characteristics of the two groups are listed in Table 1. The mean baseline VA in the IVB group was significantly better than that in the triple-therapy group ($P = 0.038$). Seventy-five patients in the IVB group and 66 patients in the triple-therapy group were followed up for more than a year after their first treatment. The mean follow-up period for the IVB group was 13.1 months (range 3.0–35.3 months); that for the triple-therapy group was 13.1 months (range 3.0–22.7 months). The mean number of treatments during the 1-year follow-up period was 2.59 (range 1–8) in the IVB group and 1.61 (range 1–5) in the triple-therapy group—the number of treatments in the triple-therapy group being significantly less than that in the IVB group ($P < 0.01$).

Figure 1 shows the mean VA changes from baseline for the IVB group and for the triple-therapy group. Members of both groups maintained vision—the mean change at 12 months from baseline being a gain of 0.026 for both groups. Although the VA in the IVB group tended to improve immediately after treatment, it had a tendency to improve more gradually in the triple-therapy group.

The genotype frequencies of the four VEGF tagging SNPs in each group are shown in Table 2. Although we chose SNPs with relatively high minor allele frequencies, there were only a few patients with the GG genotype in rs3025033 or the TT genotype in rs3025035 in the triple-therapy group; accordingly, we excluded these two SNPs from the analyses.

We examined first the differences in initial VA among the genotypes of rs699946 in the IVB and triple-therapy groups. Table 3 shows demographic characteristics by genotypes of rs699946 in each group. There was no significant difference in mean baseline VA among AA, AG, and GG genotypes in either group ($P = 0.101$ and 0.433, respectively). We evaluated next the changes in VA after treatment in each group; these changes are shown in Fig. 2. As depicted in this figure, the VA seemed to improve continuously in the patients with the GG genotype, whereas it did not change appreciably during the follow-up period in the patients with the AG or AA genotypes in either treatment group. When the mean VA at 12 months was examined, it was significantly different among the three genotypes in both treatment groups ($P = 0.025$ and 0.010, respectively). Furthermore, when we examined the trend in VA changes at 12 months among these three genotypes, the G allele showed a significant trend toward better visual acuity changes in both the IVB group ($P = 0.044$) and the triple-therapy group ($P = 0.010$). Visual acuity changes at 12 months were best in those with the GG genotype,

Table 1 Characteristics of the study population

	Bevacizumab	Triple therapy	*P* value
Number of patients	94	79	–
Mean age (years)	74.9	75.5	0.60
Female (%)	31.9%	26.6%	0.26
Right eye (%)	50.0%	46.8%	0.42
Mean baseline VA	0.546	0.631	0.038
Mean follow-up (months)	13.1	13.1	0.87

VA visual acuity

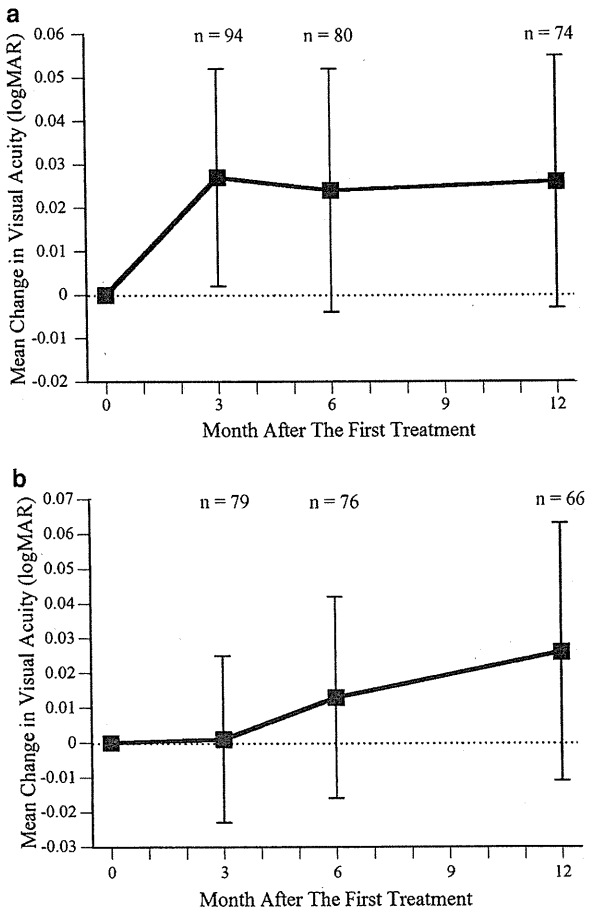

Fig. 1 Visual acuity over time for the IVB and triple-therapy groups. **a** Visual acuity (VA) over time in patients treated with intravitreal bevacizumab alone (IVB group) and, **b** in patients treated with photodynamic therapy with IVB and intravitreal triamcinolone acetonide (triple-therapy group) who were followed up for more than a year after their first treatment. Both show the mean VA change ± SEM in logMAR from baseline

middle in those with the GA genotype, and worst in those with the AA genotype. We evaluated whether rs699946 is also associated with visual prognosis after the treatment in the subgroups of PCV and typical AMD. We found the same tendency for the visual prognosis in both subgroups, although most of the analyses did not reach a significant level because of the small sample size (data not shown).

Next, we evaluated whether there were significant differences in the number of treatments, incidences of recurrence, or the periods until recurrence according to the VEGF rs699946 genetic variant using the patients who had been followed for 1 year or longer. During the 1-year follow-up period, there was no significant difference in the number of any of the treatments (intravitreal anti-VEGF drug, PDT, and combined therapy) among the three genotypes in either group ($P = 0.878$ and 0.477, respectively); contents of additional treatments (whether or not PDT was performed as additional therapy) did not differ among the two groups (Table 4). In the IVB patients who underwent one to three injections as the initial treatment, there was no significant difference in the number of injections used as the initial treatment among the three genotypes (AA 1.41, AG 1.57, GG 1.64, $P = 0.627$). There was also no significant difference in the frequency of recurrence ($P = 0.431$ and 0.342, respectively) or the period until it occurred ($P = 0.612$ and 0.980, respectively) among the three genotypes of either group (Table 5).

We examined the initial VA and that after treatment for all eyes in both the IVB group and the triple-therapy group based on the presence of rs699947. There was no significant difference in the mean baseline VA among the rs699947 AA, AC, and CC genotypes in either group ($P = 0.820$ and 0.691, respectively). Although the mean VA seemed to change notably in the rs699947 AA genotype whereas it did not change appreciably during the follow-up period in the other two genotypes (AC and CC) (Fig. 3), we found no relationship among these three genotypes and visual acuity in either group ($P = 0.257$ and 0.100, respectively). There was no difference in the frequency of AMD recurrence ($P = 0.645$ and 0.697, respectively) or the period until it was noted ($P = 0.987$ and 0.423, respectively) among the three rs699947 genotypes in either group.

Table 2 Distribution in the study population

Genotype, *n* (%)	Bevacizumab ($n = 94$)	Triple therapy ($n = 79$)
rs699946	$n = 91$	$n = 78$
AA	22 (24.2)	26 (33.3)
AG	47 (51.6)	44 (56.4)
GG	22 (24.2)	8 (10.3)
rs699947	$n = 92$	$n = 79$
AA	4 (4.3)	5 (6.3)
AC	33 (35.9)	37 (46.8)
CC	55 (59.8)	37 (46.8)
rs3025033	$n = 92$	$n = 79$
AA	65 (70.7)	63 (79.7)
AG	23 (25.0)	15 (19.0)
GG	4 (4.3)	1 (1.3)
rs3025035	$n = 92$	$n = 79$
CC	54 (58.7)	45 (57.0)
CT	31 (33.7)	31 (39.2)
TT	7 (7.6)	3 (3.8)

Discussion

In this study, VEGF rs699946 SNP was associated significantly with the visual prognosis of AMD after treatment with either IVB alone or after triple therapy. By evaluating the SNP before treatment, patients with neovascular AMD will be able to know what to expect after treatment, including what anti-VEGF drugs will be applicable. Recently, intensive studies have been performed on the association between various SNPs and the response to treatment of patients with AMD. Among the SNPs studied,

Table 3 Demographic characteristics by genotypes of VEGF rs699946

Group	Genotype	Mean age (years)	Female (%)	Right eye (%)	Mean follow-up (months)	Pretreatment VA	*P* value*
Bevacizmab	AA	74.9	9.1	54.5	14.2	0.659	0.101
	AG	74.8	36.2	46.8	12.6	0.493	
	GG	74.9	45.5	45.5	11.9	0.496	
Triple therapy	AA	75.4	23.1	61.5	12.9	0.684	0.4326
	AG	77.0	29.5	34.1	13.1	0.591	
	GG	75.2	12.5	62.5	14.1	0.628	

VA visual acuity

* The *P* values were generated by the ANOVA test

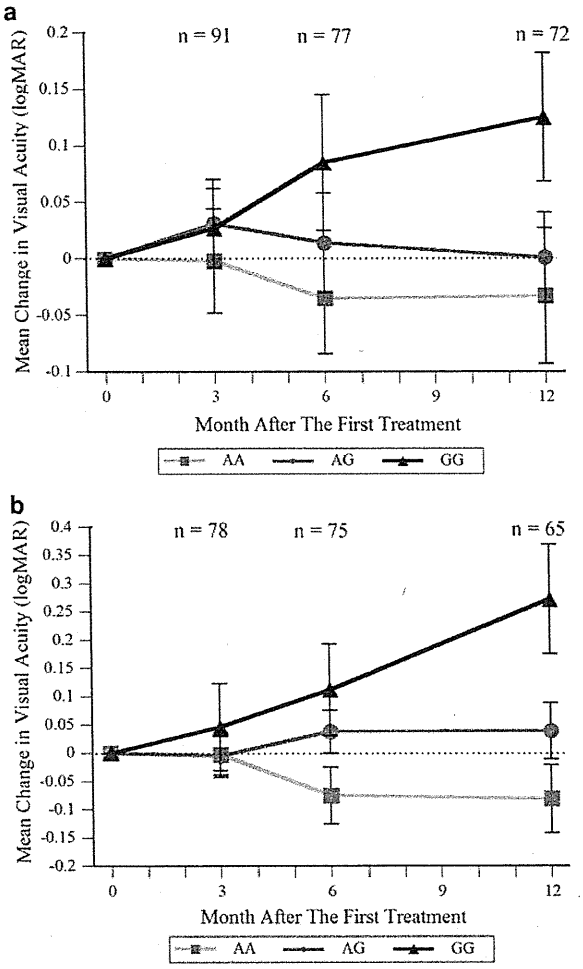

Fig. 2 Visual prognosis by VEGF rs699946 for the IVB and triple-therapy groups. The *two panels* show visual acuity (VA) over time in **a** the patients treated with intravitreal bevacizumab alone (IVB group) and, **b**, in the patients treated with photodynamic therapy with IVB and intravitreal triamcinolone acetonide (triple-therapy group). *Both graphs* show the mean VA changes ± SEM in logMAR from baseline among the three genotypes of VEGF rs699946 (*squares* AA, *circles* AG, and *triangles* GG). There was no difference in the mean baseline VA among the genotypes in either group. The G allele showed a significant trend toward better visual acuity in both the IVB group and in the triple-therapy group at 12 months ($P = 0.044$ and 0.010, respectively)

CFH Y402H was shown to correlate with the response to PDT, IVB, and ranibizumab [28–30]. These studies encourage us to personalize the treatment for each individual patient, with most suitable treatment being determined by studying the genotypes of each patient. However, the Y402H polymorphism is extremely rare in East Asia [31–36]; which markedly affects its applicability. Because the minor allele frequency of rs699946 was 43.9% in this study, this polymorphism is an attractive candidate for personalized treatment of AMD.

If the risk allele of an SNP is associated with VA prognosis, this risk allele frequency should have a trend. Because the risk-homo genotype has two risk alleles, it should have the worst prognosis, whereas the non-risk-homo genotype which contains no risk allele should have the best prognosis. Accordingly, this genotype, which contains one risk allele should have a "middle of the road" prognosis. Although CFH Y402H is a strong susceptibility gene polymorphism for AMD, the trend in the association between its risk allele and the response to treatment is not clear. Indeed, most reports show that the visual outcome is not always the best with the non-risk-homo genotype (TT) or the worst with the risk-homo genotype (CC). Goverdhan et al. [28] showed that those with a hetero genotype (TC) have the best VA changes after PDT for AMD, compared with those with the risk-homo genotype (CC) or the non-risk-homo genotype (TT). Similarly, Brantley et al. [30] reported that final visual acuity is better in those with the TC genotype than in those with the CC or TT genotypes. They reported that, when treated with IVB, AMD eyes with the TC genotype have a better visual prognosis than those with the CC genotype, and that the visual prognosis is almost the same for those with the TC and TT genotypes [29].

Unlike CFH Y402H, VEGF rs699946 SNP showed a clear trend in that, after treatment for AMD, visual prognosis was best with the GG genotype, medium with the GA genotype, and worst with the AA genotype. The frequency of the risk allele G would contribute to better prognosis. This association of the VEGF gene polymorphisms with visual prognosis in eyes with AMD seems to be inconsistent with previous studies that showed no association between AMD and VEGF gene polymorphisms [25, 37, 38]. At the same time, it does seem natural that the disease-susceptibility gene is different from the gene associated with the response to treatment. VEGF gene polymorphism may well contribute to the progress of AMD, rather than to the onset of AMD.

Although rs699946 has not been studied in depth, a recent report showed that the genotype of rs699946 was associated significantly with severe diabetic retinopathy [39]. In both diabetic retinopathy and AMD, it is well-known that VEGF contributes to pathologic neovascularization and to retinal edema. The association of rs699947, which, like rs699946, is on the promoter region, with the occurrence of diseases or with their prognosis has been investigated in various organs [24, 40–43]. The association of rs699947 and AMD has been denied in reports by Boekhoorn et al. [38] and by Lin et al. [10], whereas haplotype analysis did show an association of rs699947 with AMD [44]. Recently, Immonen et al. [25] showed that the frequency of rs699947 is significantly different in PDT nonresponders than in PDT responders. However, they did not evaluate its association to visual prognosis. In this

Table 4 Number and content of treatments during 1-year follow-up

Genotype	Number of treatments	*P* value*	Number of additional treatments with PDT	*P* value*
Intravitreal bevacizmab				
AA	2.52	0.878	0.05	0.658
AG	2.67		0.03	
GG	2.47		0.00	
Triple therapy				
AA	1.80	0.477	0.19	0.993
AG	1.64		0.18	
GG	2.17		0.17	

* The *P* values were generated by the ANOVA test

Table 5 Results from evaluation for recurrence

Genotype	Recurrence		*P* value (chi-squared)	Period until recurrence (days)	*P* value (ANOVA)
	+	−			
Intravitreal bevacizmab					
AA	9	12	0.431	171	0.612
AG	18	15		213	
GG	12	7		172	
Triple therapy					
AA	8	13	0.342	212	0.980
AG	21	17		213	
GG	2	4		194	

study, rs699947 did not affect visual prognosis after IVB or triple therapy for AMD but, because we had only four patients treated with IVB who had the AA genotype of rs699947 and five patients treated with triple therapy who had the AA genotype of rs699947, a larger cohort might show an association of rs699947 with visual prognosis. However, rs699946 would be the better genotype to be used clinically for personalized medicine because its distribution is more balanced than is that of rs699947.

The VEGF rs699946 is 5.8 kb upstream of the 5′ transcription start sites. The VEGF rs699946 captures and reflects one SNP on the promoter region (rs833060) and four SNPs on the VEGF gene (rs833068, rs833069, rs3024997, rs3025000) with high linkage disequilibrium. Because some of these SNPs correlate with VEGF production [45], a VEGF genotype might affect visual prognosis via the amount of VEGF produced. In addition to the amount of VEGF, the ratio of various VEGF isoforms can affect the prognosis of AMD because each VEGF isoform has its own role in both pathologic and physiologic neovascularization [46]. Considering that rs699946 exists upstream of the 5′ transcription start sites, it may affect splicing of VEGF and result in a changes in the expression level of VEGF isotypes such as $VEGF_{121}$, $VEGF_{165}$, and $VEGF_{189}$.

It might seem surprising that VEGF rs699946 SNP affected the visual outcome of eyes with AMD after two different treatments: IVB alone and triple therapy. Because the objective of IVB treatment is to eradicate CNV and to attenuate the exudative changes by suppressing VEGF, it seems plausible that variations in the VEGF gene change the visual outcome after treatment. However, the action of VEGF and IVB in triple therapy may be more complex. It was thought that IVTA and IVB suppress the VEGF upregulation that is induced by PDT [12]. Moreover, IVB may have a direct effect on eradication of CNV and on attenuation of the exudative change. Both of these mechanisms would lead to association of the VEGF gene variation with the visual outcome after triple therapy, but further studies are needed to clarify the biological functions of these VEGF genetic variants. However, because either anti-VEGF drugs alone or combined treatment that includes PDT with anti-VEGF drugs are currently the main treatment modalities for AMD, our findings of an association between VEGF gene polymorphism and the visual outcome after both IVB and triple therapy seem helpful.

In this study, VA in the IVB group tended to improve immediately after treatment whereas it tended to improve more gradually in the triple-therapy group. The Mont Blanc study shows that patients treated with IVB alone had better VA than patients treated with PDT + IVB. Furthermore, recent randomized clinical trials have shown that patients treated with IVB had a significantly better VA outcome than those treated with PDT + IVTA [47]. It can be

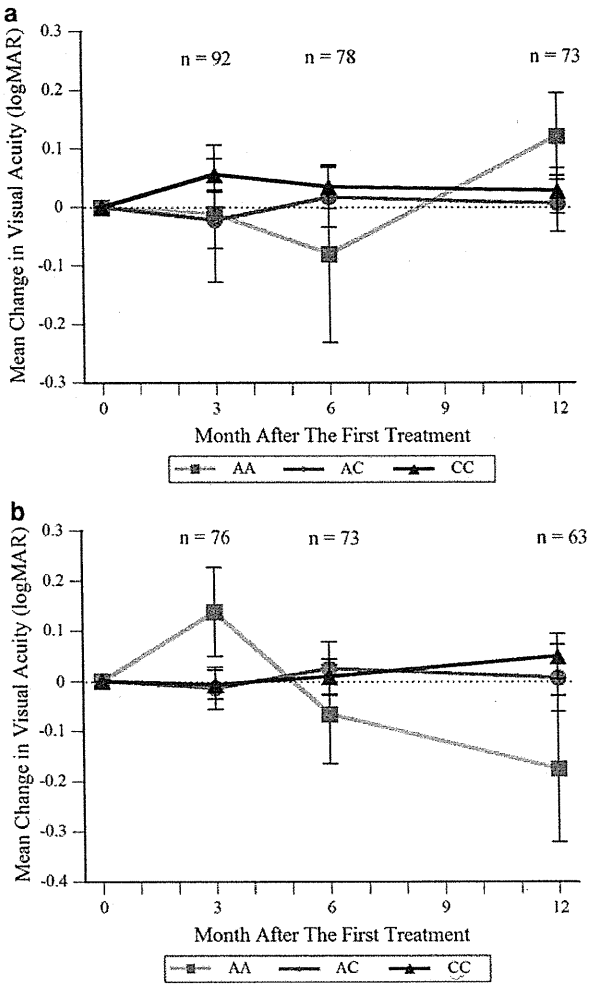

Fig. 3 Visual prognosis by VEGF rs699947 for the IVB and triple-therapy groups. **a** Visual acuity (VA) over time in the patients treated with intravitreal bevacizumab alone (IVB group) and, **b**, in the patients treated with photodynamic therapy with IVB and intravitreal triamcinolone acetonide (triple-therapy group). *Both graphs* show the mean VA changes ± SEM in logMAR from baseline among three genotypes of VEGF rs699947 rs699946 (*squares* AA, *circles* AC, and *triangles* CC). There was no difference in the mean baseline VA among the genotypes in either group. No relationship was seen among these three genotypes for visual acuity in either group ($P = 0.257$ and 0.100, respectively)

suggested that PDT and IVTA may delay the vision recovery even when we take into account the fact that the initial visual acuity was significantly different between the IVB group and the triple-therapy group in this study.

This retrospective study is limited by the size of the patient cohort and, although we selected tag SNPs with relatively high minor allele frequency, we could not evaluate the effects of some SNPs on visual prognosis. Because there were only a few patients with the GG genotype in rs3025033 and with the TT genotype in rs3025035 in the triple-therapy group, further investigation with a larger patient cohort may enable better evaluation of gene interactions and their relationship with treatment response. A further limitation of this study is the lack of evaluation of visual prognosis in the AMD patients without any treatment. Patients with the G allele in VEGF rs699946 might have better visual prognosis without treatment. In addition, the treatment method was not randomly assigned or chosen to follow solid criteria, which should be considered as a bias when interpreting our findings. Hidden baseline characteristics of the participants might affect the visual outcomes after treatment. The baseline VA of the patients with the AA genotype of rs699946 was slightly worse in both groups. Because the visual changes depended on the baseline VA, we cannot exclude the possibility that the differences of the baseline VA might affect the results of this study, even taking into account that they were not statistically significant. However, in this study, the rs699946 genotype was associated with the visual prognosis after both treatments. Further studies, for example a prospective study, would be needed to confirm the association between these variants and the visual prognosis of AMD.

Anti-VEGF drugs have become the principal treatment of neovascular AMD because the visual results are reported to be better than those obtained with PDT. However, numerous injections of the anti-VEGF drug may be required to maintain those visual benefits. To reduce the number of reinjections of anti-VEGF drugs, combination therapy, for example the triple therapy reported herein, has been evaluated. Because the rs699946 polymorphisms of the VEGF gene were associated with visual outcomes after both IVB and triple therapy, determination of the genotype of rs699946 can be of great help in predicting the visual outcome of AMD after treatment.

Acknowledgments The authors wish to thank Drs Norimoto Gotoh, Hisako Hayashi, Sotaro Ooto, and Hiroshi Tamura for their valuable contributions to this study. This study was supported in part by Grants-in-aid for scientific research (nos. 21249084 and 200791294) from the Japan Society for the Promotion of Science, Tokyo, Japan, and the Japan National Society for the Prevention of Blindness, Tokyo, Japan.

References

1. Brown MM, Brown GC, Sharma S, Stein JD, Roth Z, Campanella J, et al. The burden of age-related macular degeneration: a value-based analysis. Curr Opin Ophthalmol. 2006;17:257–66.
2. Photodynamic therapy of subfoveal choroidal neovascularization in age-related macular degeneration with verteporfin: one-year results of 2 randomized clinical trials—TAP report. Treatment of age-related macular degeneration with photodynamic therapy (TAP) Study Group. Arch Ophthalmol. 1999;117:1329–45.
3. Gragoudas ES, Adamis AP, Cunningham ET Jr, Feinsod M, Guyer DR. Pegaptanib for neovascular age-related macular degeneration. N Engl J Med. 2004;351:2805–16.

4. Chakravarthy U, Adamis AP, Cunningham ET, Jr, Goldbaum M, Guyer DR, Katz B, et al. Year 2 efficacy results of 2 randomized controlled clinical trials of pegaptanib for neovascular age-related macular degeneration. Ophthalmology. 2006;113:1508 e1–25.
5. Michels S, Rosenfeld PJ, Puliafito CA, Marcus EN, Venkatraman AS. Systemic bevacizumab (Avastin) therapy for neovascular age-related macular degeneration twelve-week results of an uncontrolled open-label clinical study. Ophthalmology. 2005;112:1035–47.
6. Rosenfeld PJ, Brown DM, Heier JS, Boyer DS, Kaiser PK, Chung CY, et al. Ranibizumab for neovascular age-related macular degeneration. N Engl J Med. 2006;355:1419–31.
7. Avery RL, Pieramici DJ, Rabena MD, Castellarin AA, Nasir MA, Giust MJ. Intravitreal bevacizumab (Avastin) for neovascular age-related macular degeneration. Ophthalmology. 2006;113: 363–72 e5.
8. Heier JS, Antoszyk AN, Pavan PR, Leff SR, Rosenfeld PJ, Ciulla TA et al. Ranibizumab for treatment of neovascular age-related macular degeneration: a phase I/II multicenter, controlled, multidose study. Ophthalmology. 2006;113:633 e1–4.
9. Lopez PF, Sippy BD, Lambert HM, Thach AB, Hinton DR. Transdifferentiated retinal pigment epithelial cells are immunoreactive for vascular endothelial growth factor in surgically excised age-related macular degeneration-related choroidal neovascular membranes. Invest Ophthalmol Vis Sci. 1996;37: 855–68.
10. Kvanta A, Algvere PV, Berglin L, Seregard S. Subfoveal fibrovascular membranes in age-related macular degeneration express vascular endothelial growth factor. Invest Ophthalmol Vis Sci. 1996;37:1929–34.
11. Frank RN, Amin RH, Eliott D, Puklin JE, Abrams GW. Basic fibroblast growth factor and vascular endothelial growth factor are present in epiretinal and choroidal neovascular membranes. Am J Ophthalmol. 1996;122:393–403.
12. Yip PP, Woo CF, Tang HH, Ho CK. Triple therapy for neovascular age-related macular degeneration using single-session photodynamic therapy combined with intravitreal bevacizumab and triamcinolone. Br J Ophthalmol. 2009;93:754–8.
13. Ahmadieh H, Taei R, Soheilian M, Riazi-Esfahani M, Karkhaneh R, Lashay A, et al. Single-session photodynamic therapy combined with intravitreal bevacizumab and triamcinolone for neovascular age-related macular degeneration. BMC Ophthalmol. 2007;7:10.
14. Tammela T, Enholm B, Alitalo K, Paavonen K. The biology of vascular endothelial growth factors. Cardiovasc Res. 2005;65: 550–63.
15. Renner W, Kotschan S, Hoffmann C, Obermayer-Pietsch B, Pilger EA. Common 936 C/T mutation in the gene for vascular endothelial growth factor is associated with vascular endothelial growth factor plasma levels. J Vasc Res. 2000;37:443–8.
16. Awata T, Inoue K, Kurihara S, Ohkubo T, Watanabe M, Inukai K, et al. A common polymorphism in the 5′-untranslated region of the VEGF gene is associated with diabetic retinopathy in type 2 diabetes. Diabetes. 2002;51:1635–9.
17. Watson CJ, Webb NJ, Bottomley MJ, Brenchley PE. Identification of polymorphisms within the vascular endothelial growth factor (VEGF) gene: correlation with variation in VEGF protein production. Cytokine. 2000;12:1232–5.
18. Petrovic MG, Korosec P, Kosnik M, Osredkar J, Hawlina M, Peterlin B, et al. Local and genetic determinants of vascular endothelial growth factor expression in advanced proliferative diabetic retinopathy. Mol Vis. 2008;14:1382–7.
19. Krippl P, Langsenlehner U, Renner W, Yazdani-Biuki B, Wolf G, Wascher TC, et al. A common 936 C/T gene polymorphism of vascular endothelial growth factor is associated with decreased breast cancer risk. Int J Cancer. 2003;106:468–71.
20. Diao LP, Yu XM, Gao YH, Li Y, Liu HS, Liu LH, et al. Association of VEGF genetic polymorphisms with the clinical characteristics of non-Hodgkin's lymphoma. J Cancer Res Clin Oncol. 2009;135:1473–81.
21. Zarbock R, Hendig D, Szliska C, Kleesiek K, Gotting C. Vascular endothelial growth factor gene polymorphisms as prognostic markers for ocular manifestations in pseudoxanthoma elasticum. Hum Mol Genet. 2009;18:3344–51.
22. Girnita DM, Brooks MM, Webber SA, Burckart GJ, Ferrell R, Zdanowicz G, et al. Genetic polymorphisms impact the risk of acute rejection in pediatric heart transplantation: a multi-institutional study. Transplantation. 2008;85:1632–9.
23. Kim JG, Chae YS, Sohn SK, Cho YY, Moon JH, Park JY, et al. Vascular endothelial growth factor gene polymorphisms associated with prognosis for patients with colorectal cancer. Clin Cancer Res. 2008;14:62–6.
24. Kim DH, Lee NY, Lee MH, Sohn SK, Do YR, Park JY. Vascular endothelial growth factor (VEGF) gene (VEGFA) polymorphism can predict the prognosis in acute myeloid leukaemia patients. Br J Haematol. 2008;140:71–9.
25. Immonen I, Seitsonen S, Tommila P, Kangas-Kontio T, Kakko S, Savolainen ER et al. Vascular endothelial growth factor gene variation and the response to photodynamic therapy in age-related macular degeneration. Ophthalmology. 2009.
26. Thorisson GA, Smith AV, Krishnan L, Stein LD. The International HapMap Project Web site. Genome Res. 2005;15:1592–3.
27. Bewick V, Cheek L, Ball J. Statistics review 10: further nonparametric methods. Crit Care. 2004;8:196–9.
28. Goverdhan SV, Hannan S, Newsom RB, Luff AJ, Griffiths H, Lotery AJ. An analysis of the CFH Y402H genotype in AMD patients and controls from the UK, and response to PDT treatment. Eye. 2008;22:849–54.
29. Brantley MA Jr, Fang AM, King JM, Tewari A, Kymes SM, Shiels A. Association of complement factor H and LOC387715 genotypes with response of exudative age-related macular degeneration to intravitreal bevacizumab. Ophthalmology. 2007;114: 2168–73.
30. Brantley MA Jr, Edelstein SL, King JM, Plotzke MR, Apte RS, Kymes SM, et al. Association of complement factor H and LOC387715 genotypes with response of exudative age-related macular degeneration to photodynamic therapy. Eye. 2009;23: 626–31.
31. Lee KY, Vithana EN, Mathur R, Yong VH, Yeo IY, Thalamuthu A, et al. Association analysis of CFH, C2, BF, and HTRA1 gene polymorphisms in Chinese patients with polypoidal choroidal vasculopathy. Invest Ophthalmol Vis Sci. 2008;49:2613–9.
32. Gotoh N, Yamada R, Hiratani H, Renault V, Kuroiwa S, Monet M, et al. No association between complement factor H gene polymorphism and exudative age-related macular degeneration in Japanese. Hum Genet. 2006;120:139–43.
33. Fuse N, Miyazawa A, Mengkegale M, Yoshida M, Wakusawa R, Abe T, et al. Polymorphisms in complement factor H and hemicentin-1 genes in a Japanese population with dry-type age-related macular degeneration. Am J Ophthalmol. 2006;142:1074–6.
34. Uka J, Tamura H, Kobayashi T, Yamane K, Kawakami H, Minamoto A, et al. No association of complement factor H gene polymorphism and age-related macular degeneration in the Japanese population. Retina. 2006;26:985–7.
35. Okamoto H, Umeda S, Obazawa M, Minami M, Noda T, Mizota A, et al. Complement factor H polymorphisms in Japanese population with age-related macular degeneration. Mol Vis. 2006;12:156–8.
36. Mori K, Gehlbach PL, Kabasawa S, Kawasaki I, Oosaki M, Iizuka H, et al. Coding and noncoding variants in the CFH gene and cigarette smoking influence the risk of age-related macular degeneration in a Japanese population. Invest Ophthalmol Vis Sci. 2007;48:5315–9.
37. Richardson AJ, Islam FM, Guymer RH, Cain M, Baird PN A. Tag-single nucleotide polymorphisms approach to the vascular

endothelial growth factor-A gene in age-related macular degeneration. Mol Vis. 2007;13:2148–52.
38. Boekhoorn SS, Isaacs A, Uitterlinden AG, van Duijn CM, Hofman A, de Jong PT, et al. Polymorphisms in the vascular endothelial growth factor gene and risk of age-related macular degeneration: the Rotterdam Study. Ophthalmology. 2008;115:1899–903.
39. Abhary S, Burdon KP, Gupta A, Lake S, Selva D, Petrovsky N, et al. Common sequence variation in the VEGFA gene predicts risk of diabetic retinopathy. Invest Ophthalmol Vis Sci. 2009;50:5552–8.
40. Kim DH, Xu W, Kamel-Reid S, Liu X, Jung CW, Kim S et al. Clinical relevance of vascular endothelial growth factor (VEGFA) and VEGF receptor (VEGFR2) gene polymorphism on the treatment outcome following imatinib therapy. Ann Oncol. 2009.
41. Del Bo R, Ghezzi S, Scarpini E, Bresolin N, Comi GP. VEGF genetic variability is associated with increased risk of developing Alzheimer's disease. J Neurol Sci. 2009;283:66–8.
42. Brown DM, Kaiser PK, Michels M, Soubrane G, Heier JS, Kim RY, et al. Ranibizumab versus verteporfin for neovascular age-related macular degeneration. N Engl J Med. 2006;355:1432–44.
43. Kong SY, Park JW, Lee JA, Park JE, Park KW, Hong EK, et al. Association between vascular endothelial growth factor gene polymorphisms and survival in hepatocellular carcinoma patients. Hepatology. 2007;46:446–55.
44. Perrin RM, Konopatskaya O, Qiu Y, Harper S, Bates DO, Churchill AJ. Diabetic retinopathy is associated with a switch in splicing from anti- to pro-angiogenic isoforms of vascular endothelial growth factor. Diabetologia. 2005;48:2422–7.
45. Pabst S, Karpushova A, Diaz-Lacava A, Herms S, Walier M, Zimmer S et al. VEGF gene haplotypes are associated with sarcoidosis. Chest. 2009.
46. Ishida S, Usui T, Yamashiro K, Kaji Y, Amano S, Ogura Y, et al. VEGF164-mediated inflammation is required for pathological, but not physiological, ischemia-induced retinal neovascularization. J Exp Med. 2003;198:483–9.
47. Sacu S, Michels S, Prager F, Weigert G, Dunavoelgyi R, Geitzenauer W, et al. Randomised clinical trial of intravitreal Avastin vs photodynamic therapy and intravitreal triamcinolone: long-term results. Eye (Lond). 2009;23:2223–7.

Macular Choroidal Thickness and Volume in Normal Subjects Measured by Swept-Source Optical Coherence Tomography

Masaya Hirata,[1] *Akitaka Tsujikawa,*[1] *Akiko Matsumoto,*[1,2] *Masanori Hangai,*[1] *Sotaro Ooto,*[1] *Kenji Yamashiro,*[1] *Masahiro Akiba,*[2] *and Nagahisa Yoshimura*[1]

Purpose. To study the choroidal thickness in healthy subjects by swept-source optical coherence tomography (SS-OCT) at longer wavelength.

Methods. The macular area of 31 eyes (31 healthy volunteers) was studied with an SS-OCT prototype system, which uses a tunable laser as a light source operated at 100,000 Hz A scan repetition rate in the 1-μm wavelength region. Three-dimensional volumetric measurement comprised of 512 × 128 A scans was acquired in 0.8 second. From a series of OCT images, a chroidal thickness map of the macular area was created by manual segmentation. To evaluate interoperator reproducibility, the choroidal thickness in each section from 10 subjects was determined independently by two observers.

Results. SS-OCT at the 1-μm wavelength region allowed visualization of the fine structure of the choroid as well as that of the retina. Mean choroidal thickness and volume in the macula area were, respectively, 191.5 ± 74.2 μm and 5.411 ± 2.097 mm^3. The mean choroidal thickness of the outer nasal area was significantly thinner than that of all other areas ($P < 0.05$). The measurements by the two independent observers were significantly identical; the intraclass correlation coefficient in mean choroidal thickness was between 0.945 and 0.980 in each area. The macular choroidal thickness was significantly correlated with axial length after adjustment for age ($P < 0.001$), and with age after adjustment for axial length ($P < 0.001$).

Conclusions. SS-OCT system at 1 μm provides macular choroidal thickness maps and allows one to evaluate the choroidal thickness more accurately. (*Invest Ophthalmol Vis Sci.* 2011; 52:4971-4978) DOI:10.1167/iovs.11-7729

So far, the thickness of the choroid has been measured by ultrasound and magnetic resonance imaging (MRI),[1,2] although their resolution of imaging within the choroid is limited.[1,2] Recently, optical coherence tomography (OCT) has been used to obtain quantitative measurements of the retinal thickness and to detect morphologic changes in the retinal architecture.[3-5] However, commercially available OCT, which functions at approximately 800 nm, can visualize the entire choroid only in eyes with high myopia[6,7] because of low penetration and high backscattering at the level of the retinal pigment epithelium (RPE).[8]

Since Spaide and associates[9] introduced enhanced depth imaging (EDI)-OCT based on spectral-domain OCT technology, an increasing number of investigators have studied the choroidal thickness in both healthy eyes and eyes with various pathologies.[10-26] In fact, EDI-OCT does allow visualization of the choroidal structure in detail and measurement of choroidal thickness.[9] However, EDI-OCT requires averaging of 50 to 100 B scans to achieve high-contrast and low-speckle noise. In most studies that have used EDI-OCT, the "choroidal thickness" is a representative value obtained at one or even several different measurement points, often at the foveal center.[10-26] However, measurement of a few sampling points tends to be influenced by focal thickening or thinning of the choroid[21,27] or, more often, by irregularity of the inner chorioscleral border.[16,17]

Recently, other investigators have reported the measurement of choroidal thickness with the use of OCT at a longer wavelength.[28-30] In these more recent studies, higher penetration of the OCT probe light, which uses a center wavelength of 1040 to 1060 nm instead of the current OCT probing light operated at approximately 800 nm, allows us to visualize the entire choroid without the EDI system or multiaveraging.[28,29] Recently, Esmaeelpour and associates[28] showed a two-dimensional (2D) choroidal thickness map with raster scan protocol using spectral-domain OCT at 1060 nm. Even more recently, Ikuno and associates[31] reported the choroidal thickness of healthy subjects measured with swept-source (SS)-OCT at 1060 nm. SS-OCT, which is characterized by a high-speed scan rate and a relatively low sensitivity roll-off versus depth compared with the spectral-domain OCT, potentially allows one to obtain a three-dimensional (3D) high-contrast image of the choroid.[32-37] However, Ikuno and associates[31] reported the choroidal thickness only at the fovea.

In using EDI-OCT or any other OCT that has a longer wavelength, the inner and outer borders of the choroid are determined manually by the observer,[9,28,31] and it is essential to estimate the error in measuring the thickness from the obtained images. In the study described herein, we scanned the macular area of healthy eyes with SS-OCT at 1050 nm, using a 3D raster scan protocol, and produced a choroidal thickness map of the macular area. By applying the grid used by the Early Treatment Diabetic Retinopathy Study (ETDRS)[38] to this map, we measured the mean choroidal thickness and volume in each area. In addition, to estimate the error in this evaluation,

From the [1]the Department of Ophthalmology and Visual Sciences, Kyoto University Graduate School of Medicine, Kyoto, Japan; and the [2]Topcon Corporation, Tokyo, Japan.

Supported, in part, by the Japan Society for the Promotion of Science, Tokyo, Japan Grant-in-Aid for Scientific Research No. 21592256, and the Japan National Society for the Prevention of Blindness, Tokyo, Japan.

Submitted for publication April 13, 2011; revised May 11, 2011; accepted May 11, 2011.

Disclosure: **M. Hirata**, None; **A. Tsujikawa**, None; **A. Matsumoto**, Topcon Corporation (E); **M. Hangai**, Topcon Corporation (C), Nidek (C); **S. Ooto**, None; **K. Yamashiro**, None; **M. Akiba**, Topcon Corporation (E); **N. Yoshimura**, Topcon Corporation (F), Nidek (F, C), Canon (F)

Corresponding author: Akitaka Tsujikawa, Department of Ophthalmology and Visual Sciences, Kyoto University Graduate School of Medicine, Sakyo-ku, Kyoto 606-8507, Japan; tujikawa@kuhp.kyoto-u.ac.jp.

interoperator reproducibility of the choroidal thickness measurements was assessed.

Materials and Methods

This prospective study consisted of 31 eyes of 31 healthy volunteers, with no ophthalmic or systemic symptoms. The macular area of these 31 eyes was examined with an SS-OCT prototype system at Kyoto University Hospital between October 2010 and February 2011. All subjects underwent a thorough ocular examination, including an autorefractometer (ARK1; Nidek, Gamagori, Japan), best-corrected visual acuity measurement with a 5-m Landolt eye chart, axial length measurement using ocular biometry (IOLMaster; Carl Zeiss Meditec, Jena, Germany), slit-lamp examination, intraocular pressure measurement, and dilated funduscopy. Exclusion criteria included history or evidence of chorioretinal or vitreoretinal diseases, including age-related macular degeneration, diabetic retinopathy, central serous chorioretinopathy, epiretinal membrane, and macular dystrophy; best-corrected visual acuity < 20/25; history of intraocular surgery; evidence of glaucoma; and poor image due to cataract or unstable fixation were also reasons for exclusion. Subjects with systemic diseases or conditions that might affect retinal or choroidal thickness were also excluded, such as those with diabetes mellitus, Vogt-Koyanagi-Harada disease, or malignant hypertension, or those who were pregnant. The Institutional Review Board and Ethics Committee of Kyoto University approved this study, which adhered to the tenets of the Declaration of Helsinki. Written informed consent was obtained from each subject before examination.

SS-OCT System and Scan Protocols

We used an SS-OCT prototype system (Topcon Corp., Tokyo, Japan) with an axial scan rate of 100,000 Hz operated at the 1-μm wavelength region. In the current SS-OCT system, the light source was a wavelength-sweeping laser with a tuning range of approximately100 nm centered at 1050 nm, yielding 8-μm axial resolution in tissue. Transverse resolution was set to approximately 20 μm. A single OCT image consisting of 1000 A lines can be acquired in 10 ms. SS-OCT imaging at 1050 nm was conducted with approximately 1 mW on the cornea, which is well below the safe retinal exposure limit established by the American National Standards Institute. Sensitivity was measured to be approximately 98 dB at this input power.

SS-OCT examinations of the eligible volunteers were performed by trained examiners after pupil dilation. A 3D imaging data set was acquired on each patient by using a raster scan protocol of 512 (horizontal) × 128 (vertical) A-scans per data set (total 65,536 axial scans/volume) in 0.8 seconds. Each 3D scan covered an area of 6 × 6-mm^2 centered on the fovea, which was confirmed by an internal-fixation and fundus camera integrated in the prototype instrument. To reduce a speckle noise, each image was denoised by applying weighted moving average from three consecutive single images. Owing to the invisible scanning light, the eye movement during 3D scan was minimal.

In each patient, fifty-times averaged horizontal and vertical scan images in 12 mm transverse scan range were obtained as well. Acquired 50 single images were registered and averaged by software to create an averaged image. The vertical scan was captured centered on the fovea while the horizontal scan was captured centered on the midpoint between fovea and optic disc.

Choroidal Thickness Measurement

The choroidal thickness was measured as the distance between the outer border of the hyper-reflective line, considered to be the RPE, and the choriosclera border. In each image of the 3D data set, lines of both RPE and the choriosclera border were determined manually by trained observers in a masked fashion. Automated built-in calibration software determined the distance between these two lines. The measurement points per image consisted of 512 points, with an interval of approximately 12 μm. From all 128 images of each 3D data set, the choroidal thickness map of 6 × 6-mm area was created.

After the choroidal thickness map was obtained, the ETDRS grid was applied to the map (Fig. 1A).[38] The ETDRS grid divides the macula into inner and outer rings, with the inner ring being 1 to 3 mm and the outer ring being 3 to 6 mm from the foveal center. The ETDRS grid divides the macula area further into superior, inferior, temporal, and nasal quadrants. Thicknesses of all measurement points within each of nine areas based on the ETDRS grid were averaged, which allowed us to obtain the mean sectorial choroidal thickness. Further, on the basis of the choroidal thickness obtained, we calculated the choroidal volume within each area in the ETDRS grid.

In the present study, choroidal thickness at a single representative point of each area of the ETDRS grid was measured manually from the 3D data set with a caliper with which the machine was equipped; these representative points were located at the center (fovea) and at 1 and 2.25 mm temporal, superior, nasal, and inferior to the macula (Fig. 1B). These representative points were located at the center of each area of the ETDRS grid. In addition, choroidal thickness at these nine points was also measured manually from multiaveraged horizontal and vertical images (Fig. 1C).

Measurement Reproducibility

In the present study, the lines of both the RPE and the choriosclera border were determined manually, in a masked fashion, by the observers. To evaluate interoperator reproducibility of these measurements, the lines of both RPE and the choriosclera border were determined independently by two observers of each scan of the 3D data set obtained from 10 subjects. Thickness maps and mean choroidal thickness within the ETDRS grid were produced independently. In these 10 subjects, choroidal thickness at a representative point of each area of the ETDRS grid was determined from the 3D data set and horizontal and vertical images were multiaveraged independently by two observ-

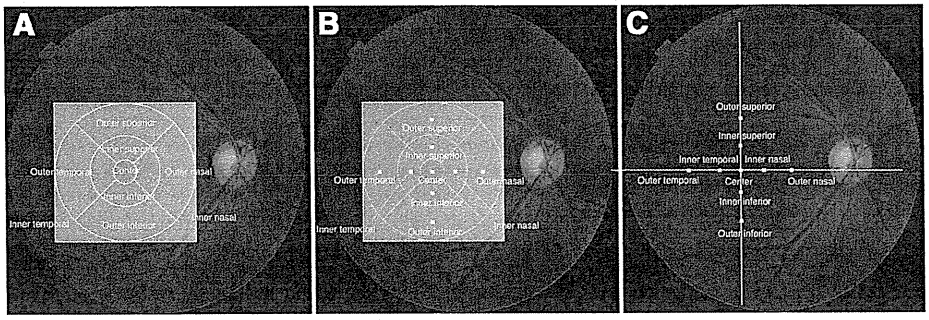

FIGURE 1. Scan protocols and areas with swept source-optical coherence tomography at 1050 nm. (A) 3D raster scan covered a 6 × 6-mm area centered on the fovea. The ETDRS grid was applied to the scanned area and mean choroidal thickness of each area was measured. (B) Representative points within the ETDRS grid were determined as center (fovea), and 1 and 2.25 mm temporal, superior, nasal, and inferior to the macula. The choroidal thickness at each representative point of each area was measured manually from a 3D data set. (C) Multiaveraged horizontal and vertical images (12-mm length) were obtained by averaging 50 scans. From these multiaveraged images, the choroidal thickness at each representative point was measured manually.

ers. The interoperator reproducibility of the choroidal thickness measurements was assessed by measuring the intraclass correlation coefficient (ICC) of each measuring procedure.

Statistical Analyses

Statistical analyses were performed by use of a commercially available software program (SPSS2: SPSS Japan, Tokyo, Japan; StatMate III: ATMS, Tokyo, Japan). All values are presented as mean ± SD. Repeated-measures ANOVA with Scheffé's test was used to compare choroidal thickness (volume) at different areas; the ICC of the choroidal thickness (volume) obtained from three different measuring procedures was also used. Pearson's correlation and partial correlation were calculated to assess the relationship of choroidal thickness of the macular area with age, refractive error, and axial length. Multiple linear regression analysis was used to evaluate the correlation between choroidal thickness of the macula and various factors. A P value < 0.05 was considered to be statistically significant.

Results

In the present study, 31 eyes of 31 healthy volunteers (14 men and 17 women), ranging in age from 21 to 87 years (64.6 ± 17.3 years), were examined. Mean refractive error was −1.67 ± 5.1 diopters (range: −9.25 to +4.25 diopters). Mean axial length was 24.6 ± 2.1 mm (range: 21.35–28.66 mm).

The SS-OCT system with a center wavelength of 1050 nm clearly showed the deep structures of the posterior pole. Because of higher penetration due to longer operating wavelength and higher scan rate (100,000 Hz) of the light source, no eye was excluded from the present study because of a low-quality image due to cataract or eye movement during the scanning procedure. Multiaveraged scans of 12 mm in length revealed structures of the retina and choroid, which allowed precise identification in all eyes of chorioscleral border beyond the vascular arcade (Fig. 2). Using a raster scan protocol with

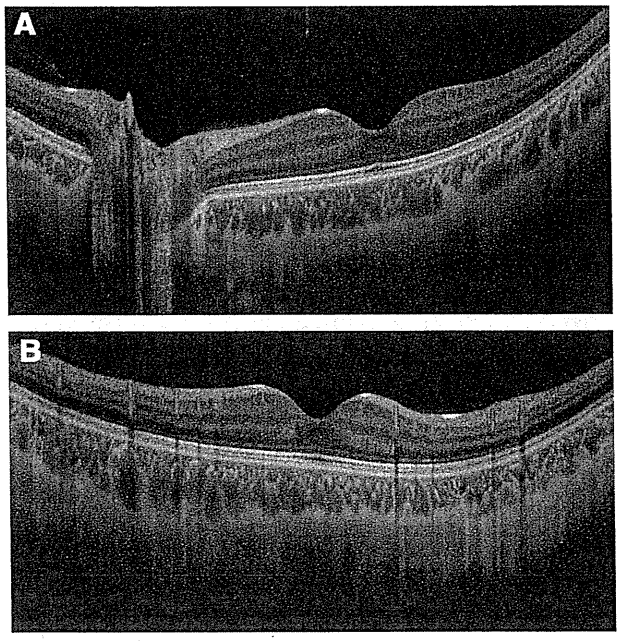

FIGURE 2. Multiaveraged horizontal (A) and vertical (B) OCT images of 12-mm length. Each image was obtained by averaging 50 single OCT images, which consisted of 1024 A scans. Fine structure from the inner limiting membrane to the chorioscleral border is seen clearly beyond the vascular arcade. Regional changes of the interface between choroid and sclera are seen.

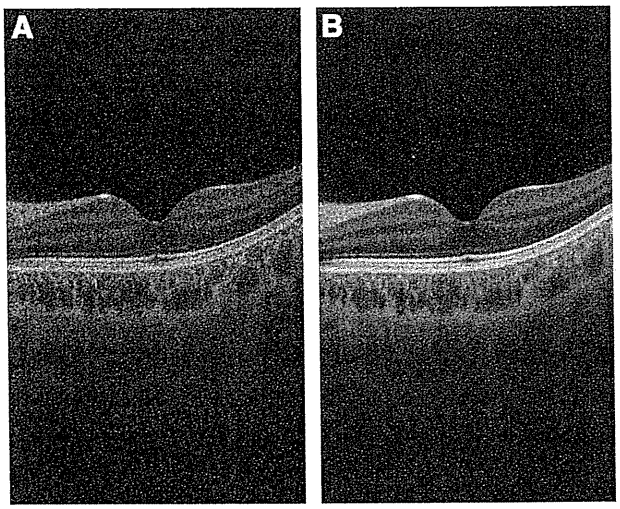

FIGURE 3. Weighted moving average applied to 3D raster scan protocol. (A) OCT image without weighted moving average. (B) OCT image with weighted moving average. In a raster scan protocol, 128 consecutive images, consisting of 512 A scans, were obtained in 0.8 second. To reduce a speckle noise, each image was enhanced by weighted moving average of three consecutive original images.

512 × 128 A scans, 3D imaging data of the 6 × 6-mm area were acquired. By weighted moving average, each image had quality sufficient to delineate both the outer border of the RPE and the chorioscleral border (Fig. 3). Based on 128 images of the 3D data set, a choroidal thickness map of the 6 × 6-mm area centered on the fovea was created for each eye (Fig. 4).

Choroidal Thickness

In our subjects, mean choroidal thickness in the macula (within a circle of 6.0-mm diameter) was 191.5 ± 74.2 μm. Table 1 shows the mean choroidal thickness of each area in the ETDRS grid as well as the choroidal thickness at a single representative point obtained from the 3D data set or multiaveraged SS-OCT images. Mean choroidal thickness within the central area was 202.6 ± 83.5 μm, which was virtually identi-

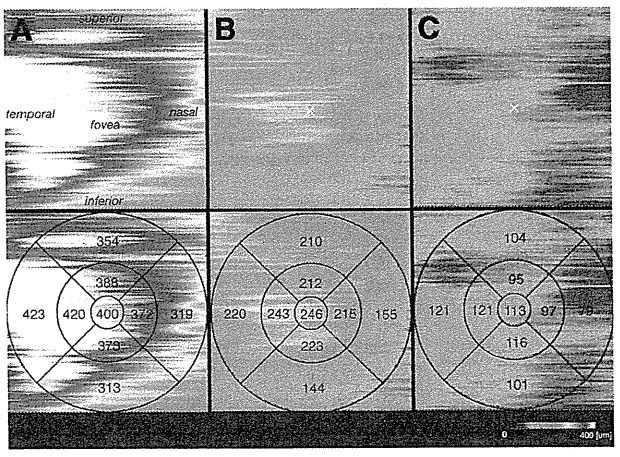

FIGURE 4. Choroidal thickness map and mean choroidal thickness of each area of the ETDRS grid. (A) Hyperopic eye (refractive error, +3.625 diopters) with an axial length of 22.91 mm. (B) Emmetropic eye (refractive error, +0.375 diopters) with a 24.16-mm axial length. (C) Myopic eye (refractive error, −9.25 diopters) with an axial length of 26.85 mm.

TABLE 1. Choroidal Thickness and Volume Obtained with Swept-Source Optical Coherence Tomography

Area	Choroidal Thickness: Mean Thickness of ETDRS Grid Area Obtained from 3D Data Set (μm)	Choroidal Thickness: Thickness at a Representative Point within ETDRS Grid Obtained from 3D Data Set (μm)	Choroidal Thickness: Thickness at a Representative Point Obtained from Multiaveraged Images (μm)	Choroidal Volume (mm^3)
Center	202.6 ± 83.5*	199.8 ± 85.6†	203.6 ± 86.1	0.159 ± 0.066
Inner temporal	204.5 ± 80.2*	201.6 ± 81.3†	197.0 ± 70.7	0.321 ± 0.126
Inner superior	206.6 ± 80.7*	206.6 ± 79.7†	205.1 ± 88.7‡	0.324 ± 0.127
Inner nasal	186.8 ± 82.0‡	183.5 ± 85.7‡	187.9 ± 79.3	0.293 ± 0.129
Inner inferior	200.4 ± 81.7†	203.9 ± 83.1†	202.2 ± 76.7	0.315 ± 0.129
Outer temporal	200.2 ± 74.3†	200.6 ± 74.0†	182.4 ± 58.9	1.061 ± 0.394†
Outer superior	215.5 ± 80.7*§	229.3 ± 86.4*§	214.0 ± 90.2‡	1.144 ± 0.428*§
Outer nasal	152.5 ± 71.1	139.6 ± 74.8	147.8 ± 73.1	0.808 ± 0.377
Outer inferior	186.0 ± 75.2‡	190.4 ± 85.9‡	185.8 ± 82.6	0.986 ± 0.398‡

* $P < 0.001$, † $P < 0.01$, ‡ $P < 0.05$, compared with values of outer nasal area. § $P < 0.05$, compared with values of outer inferior area.

cal with the foveal thickness obtained with multiaveraged SS-OCT images (203.6 ± 86.1 μm). In other areas, mean choroidal thickness was also similar to the choroidal thickness obtained from multiaveraged SS-OCT images, the difference of which was <10% in all areas.

In the present study, the nasal choroid was thinner than that of other areas; the mean thickness of the outer nasal area (152.5 ± 71.1 μm) was significantly thinner than that of all other areas ($P < 0.05$, respectively). In addition, the inferior choroid was thinner, compared with that of the superior area; the mean thickness of outer inferior area (186.0 ± 75.2 μm) was significantly thinner than that of the outer superior area (215.5 ± 80.7 μm, $P < 0.05$). Even though choroidal thickness obtained at a single point also showed a similar tendency, the differences among the values of choroidal thickness measured at a single point were less significant compared with that of mean choroidal thickness obtained with the 3D data set.

Choroidal Volume

By integrating choroidal thickness in each area, we could obtain values corresponding to the volume because of the many measurement points in the 3D data set. Table 2 shows the choroidal volume in each area. Mean choroidal volume of the center area (within a circle of 1.0-mm diameter) was 0.159 ± 0.066 mm^3, 1.412 ± 0.567 mm^3 within the inner ring (within a circle of 3.0-mm diameter), and 5.411 ± 2.097 mm^3 within the outer ring (within a circle of 6.0-mm diameter).

Interoperator Reproducibility of Choroidal Thickness Obtained by 3D SS-OCT

To evaluate interoperator reproducibility, the lines of both RPE and chorioscleral borders in each image from 10 subjects were determined independently by two observers (Fig. 5). Table 2 shows the ICC in mean choroidal thickness of each area in the ETDRS grid, as measured by the two observers. ICC in mean choroidal thickness was between 0.945 and 0.980 ($P < 0.001$). In addition, choroidal thickness at a single point obtained from multiaveraged SS-OCT images also showed a high ICC (0.945–0.985) between the two observers, which was not statistically different from the ICC in mean choroidal thickness. However, choroidal thickness at a single point of each area obtained from the 3D data set showed a high ICC (0.919–0.967), which was statistically lower than the ICC in mean choroidal thickness ($P < 0.01$) or the ICC in choroidal thickness obtained from multiaveraged SS-OCT images ($P < 0.001$).

Correlations between Age and Choroidal Thickness

Table 3 shows Pearson's correlation coefficient and partial correlation coefficient between mean choroidal thickness of

TABLE 2. Intraclass Correlation Coefficient in Choroidal Thickness from Swept-Source Optical Coherence Tomography Scans Measured by Two Observers

Area	Mean Thickness of ETDRS Grid Area Obtained from 3D Data Set: ICC	Mean Thickness of ETDRS Grid Area Obtained from 3D Data Set: P	Thickness at a Representative Point within ETDRS Grid Obtained from 3D Data Set: ICC	Thickness at a Representative Point within ETDRS Grid Obtained from 3D Data Set: P	Thickness at a Representative Point Obtained from Multiaveraged Images: ICC	Thickness at a Representative Point Obtained from Multiaveraged Images: P
Center	0.968	<0.001	0.943	<0.001	0.968	<0.001
Inner temporal	0.973	<0.001	0.953	<0.001	0.985	<0.001
Inner superior	0.961	<0.001	0.952	<0.001	0.984	<0.001
Inner nasal	0.964	<0.001	0.937	<0.001	0.978	<0.001
Inner inferior	0.958	<0.001	0.928	<0.001	0.968	<0.001
Outer temporal	0.945	<0.001	0.922	<0.001	0.945	<0.001
Outer superior	0.972	<0.001	0.967	<0.001	0.971	<0.001
Outer nasal	0.980	<0.001	0.971	<0.001	0.994	<0.001
Outer inferior	0.952	<0.001	0.919	<0.001	0.981	<0.001

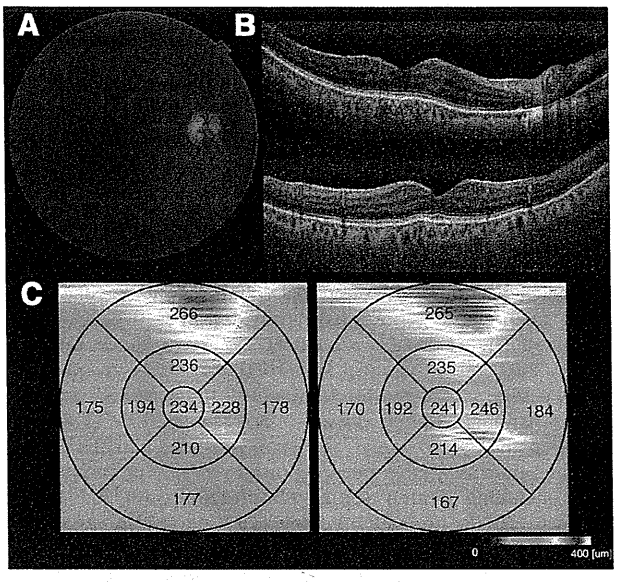

FIGURE 5. Choroidal thickness map of a healthy subject. (A) Fundus photograph of the right eye of a 77-year-old woman; visual acuity was 20/25, axial length was 22.87 mm, and refractive error was +2.0 diopters. (B) Multiaveraged horizontal (*upper*) and vertical (*lower*) images clearly show choroidal structures and the choriosclera border. The choroid seems to be thin around the optic disc and beyond the vascular arcade. (C) The choroidal thickness maps (6 × 6 mm) were measured by two independent observers and were almost identical. By applying the ETDRS grid to the map, mean choroidal thickness was obtained for each area. Choroid in the outer superior area is thicker than that of the outer lower area. In addition, there is regional thickening seen in the outer superior area and in the inner nasal area.

the macular area and age, axial length, and refractive error. The mean choroidal thickness within the macula (within the outer circle) had a weakly negative correlation with age ($r = -0.400$, $P = 0.026$) and with axial length ($r = -0.375$, $P = 0.045$), whereas it had no correlation with refractive error ($r = 0.238$, $P = 0.214$). The macular choroidal thickness was correlated significantly with age after adjustment for axial length ($r = -0.684$, $P < 0.001$) and with axial length after adjustment for age ($r = -0.684$, $P < 0.001$). In addition, similar correlations were seen in the mean choroidal thickness in the central area and within the inner circle. Table 4 shows the partial correlation coefficient between mean choroidal thickness at each quadrant and age, axial length, and refractive error. In each quadrant, choroidal thickness was negatively correlated with axial length after adjustment for age ($r = -0.720$ to -0.597, $P < 0.001$) and with age after adjustment for axial length ($r = -0.690$ to -0.613, $P < 0.001$).

Multiple Linear Regression Analysis

Table 5 shows results of the multiple linear regression analysis for mean choroidal thickness of the macula. A stepwise method was used to determine the most unexpected factors. The model determined by age and axial length had the best regression. The model showed a good coefficient of determination, which was 0.736 ($R^2 = 0.542$); the coefficients of age and axial length were -3.04 and -24.95 μm, respectively (Fig. 6).

DISCUSSION

In the present study, the macular area of healthy volunteers was viewed with a raster scan protocol in a prototype SS-OCT at 1050 nm. The tunable laser source has a longer wavelength, higher penetration, and lower scattering at the RPE than those at the conventional spectral-domain OCT operating at the 800-nm region, and thus allows for full-depth imaging of the choroid.[28–30] In addition, the tunable laser source of the SS-OCT has lower signal decay versus depth than does the existing spectral-domain OCT system.[32–37] This advantage of the SS-OCT probably allowed the clear imaging of the entire choroid within the area scanned and also allowed the highly reproducible measurements of choroidal thickness.

Importantly, high-speed scanning coupled with the high sensitivity of the SS-OCT allowed highly reproducible measurements of choroidal thickness, even in single B-scan–based imaging on a 3D raster scan protocol. In the present study, the 3D imaging data sets were acquired by using a raster scan protocol of 512 × 128 in 0.8 second. An invisible scanning line of 1-μm wavelength contributes to reduced eye motion and to patient comfort during the scan. Based on the 3D data set, we produced a 2D choroidal thickness map of the macular area for each subject and, by applying the ETDRS grid to the map, we could then obtain a mean choroidal thickness and choroidal volume in each area of the ETDRS grid. EDI-OCT is usually coupled with multiple averaging to achieve high-contrast and low-speckle noise,[9] but it does not provide as many sections as does the 3D imaging. Previously, Spaide and associates[9] reported that the choroidal thickness in the fovea of a healthy subject was 318 μm in the right eye and 335 μm in the left eye. As shown in Figure 4, choroid in the macula can show focal thickening or thinning[21,27] and, if measured from a single A scan may be influenced by irregularity or by focal indistinctness of the choriosclera border.[16,17]

TABLE 3. Pearson's Correlation Coefficient and Partial Correlation Coefficient between Mean Choroidal Thickness of the Macula Area and Age, Axial Length, and Refractive Error

Factor	Pearson's Correlation Coefficient	P	Partial Correlation Coefficient	P
Center				
Age, y	−0.282	0.125	−0.707	<0.001 (adjusted for axial length)
Axial length, mm	−0.476	0.009	−0.628	<0.001 (adjusted for age)
Refractive error, D	0.379	0.042	0.070	<0.001 (adjusted for axial length)
Within inner circle				
Age, y	−0.325	0.074	−0.647	<0.001 (adjusted for axial length)
Axial length, mm	−0.437	0.018	−0.695	<0.001 (adjusted for age)
Refractive error, D	0.322	0.089	0.006	0.978 (adjusted for axial length)
Within outer circle				
Age, y	−0.400	0.026	−0.684	<0.001 (adjusted for axial length)
Axial length, mm	−0.375	0.045	−0.684	<0.001 (adjusted for age)
Refractive error, D	0.238	0.214	−0.510	0.806 (adjusted for axial length)

TABLE 4. Partial Correlation Coefficient between Mean Choroidal Thickness of Each Quadrant and Age and Axial Length

Factor	Temporal	Superior	Nasal	Inferior	P
Age, y	−0.657	−0.672	−0.597	−0.720	<0.001 (adjustedforaxiallength)
Axial length, mm	−0.656	−0.690	−0.613	−0.678	<0.001 (adjustedfor age)

Each quadrant includes both inner and outer areas.

In the study described herein, similar to what has been reported previously,[10-26] lines of both RPE and the chorioscleral border were determined manually by the observers, so it is essential to estimate the error that may have occurred. In multiaveraged images obtained by the SS-OCT at 1050 nm, the chorioscleral border was clearly seen because of the reduction in speckle noise, even without use of the EDI system. Similar to the previous studies that used EDI-OCT,[9,11] the ICC in choroidal thickness at a single point obtained from multiaveraged images was very high (0.945-0.994). In addition, the ICC of choroidal thickness at the same point obtained from the 3D data set was sufficiently high (0.919-0.971), but was lower than the ICC of choroidal thickness at a single point obtained from multiaveraged images. Less clarity of the chorioscleral border on each image of the 3D data set compared with multiaveraged images probably accounted for less reproducibility. However, using the 3D data set, the ICC of mean choroidal thickness was also quite high (0.945-0.980). Averaging of thickness values obtained at many measurement points in each area probably contributed to minimize the error in determining choroidal thickness at each point.

To date, there have been several reports of the foveal choroidal thickness in normal eyes obtained by use of various systems.[9,11,23,28,31,39,40] This has been reported to be between 272 and 448 μm in healthy eyes. In the present study, mean choroidal thickness in the macula (within a circle of 6.0-mm diameter) was 191.5 ± 74.2 μm, and thickness in the nasal quadrant (152.5 ± 71.1 μm) was less than that in the other quadrants. In addition, the choroid in the outer superior area (215.5 ± 80.7 μm) was thicker than that in the outer inferior area (186.0 ± 75.2 μm). In our study, the subfoveal choroidal thickness was comparable to that in the superior temporal quadrant, whereas it was greater than that in the inferior nasal quadrant.

The subfoveal choroidal thickness was less than that reported previously,[9,11,23,28,31,39,40] although age of eligible subjects may be involved in this difference. The average age was much higher (64.6 ± 17.3 years) than that in previous studies (33.4-55.5 years).[9,11,23,28,31,39,40] Margolis and Spaide[11] reported that increasing age was correlated significantly with decreasing choroidal thickness, and regression analysis suggested that the subfoveal choroidal thickness decreased by 15.6 μm for each decade of life. In addition, it has been reported that different spectral-domain OCT instruments provide different retinal thickness values,[41] and this lack of interchangeability among OCT systems may also be responsible for the difference seen.

TABLE 5. Multiple Linear Regression Analysis for Choroidal Thickness of the Macula* by Axial Length and Age

Factor	Coefficient	P	SE
Intercept	1001.70	<0.001	153.50
Age, y	−3.04	<0.001	0.64
Axial length, mm	−24.95	<0.001	5.20

$R = 0.736$; $R^2 = 0.542$.

* Macular choroidal thickness = 1099.3 − 3.05 × Age − 28.53 × Axial length.

In the present study, 3D imaging of the choroid using SS-OCT allowed calculation of the choroidal volume of the macular area. So far, no previous reports have provided in vivo data on the volume of the choroid.[42] Choroidal volume reflects vascular changes such as the vascular hyperpermeability or vasodilation seen in central serous chorioretinopathy,[43] the inflammation seen in Vogt-Koyanagi-Harada disease,[44] and the decrease of vessels seen in pathologic myopia[45]; moreover, changes in the foveal choroidal thickness have been reported recently in various diseases, including central serous chorioretinopathy,[14,25] Vogt-Koyanagi-Harada disease,[13,18] polypoidal choroidal vasculopathy,[16,17] and age-related macular degeneration.[16,17] Maruko and associates[14,26] reported that choroidal thickness in the fovea becomes decreased after photodynamic therapy. In their studies, foveal choroidal thickness reflected pathophysiology of the choroid after treatment. However, still more information may be obtained by the evaluation of choroidal volume. In the present study, we applied the ETDRS grid only to the choroidal thickness maps. With some modification of the algorithm, choroidal volume within arbitrary areas could be obtained (e.g., choroidal volume within the laser-irradiated area to which photodynamic therapy is to be applied).

Previously, Ikuno and associates[31] reported that foveal choroidal thickness is weakly correlated with age ($R^2 = 0.04$), axial length ($R^2 = 0.06$), and refractive error ($R^2 = 0.046$); in the present study, mean choroidal thickness in the macula had a negative correlation with age ($r = -0.400$) and with axial length ($r = -0.375$), whereas it had no correlation with refractive error ($r = 0.238$). In addition, the correlation with age became more significant with an adjustment for axial length ($r = -0.684$), and the correlation with axial length became more significant with an adjustment for age ($r = -0.684$). However, whereas the central choroidal thickness showed a weak correlation with refractive error ($r = 0.379$), no correlation was seen after adjustment for axial length ($r = 0.070$). There have been some previous reports of a correlation between choroidal thickness and refractive er-

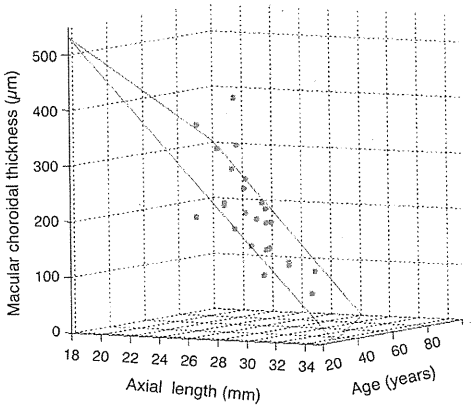

FIGURE 6. Scatterplot of macular choroidal thickness, age, and axial length. The model shows a good coefficient of determination ($R^2 = 0.542$). Macular choroidal thickness = 1099.3 − 3.05 × Age − 28.53 × Axial length.

ror,[6,20,31] and it is possible that axial length or age has some influence on this correlation. Using stepwise multiple regression analysis, we showed with great accuracy (R^2 = 0.542) that the choroidal thickness in the macula is determined by age and axial length, so it is essential that both age and axial length be taken into account when choroidal thickness is evaluated. After this model is modified and its accuracy is confirmed in future studies, it may serve to compare the macular choroidal thickness in eyes of different ages and with different axial lengths.

Compared with spectral-domain OCT at approximately 800 nm, SS-OCT at longer wavelength is reported to provide superior visualization of the posterior pole in cataractous eyes.[28,31] In the present study with SS-OCT at 1050 nm, no eyes were excluded because of poor images due to cataract. However, the present study does have many limitations. Primary among these is that it consisted of only Japanese subjects; thus, choroidal thickness and volume need to be confirmed in other ethnic groups. In addition, the small sample size might be insufficient to evaluate the mean choroidal thickness (volume) in normal eyes. In the present study, the line of RPE and the chorioscleral border were determined manually. The raster scan protocol with over 60,000 measurement points may have minimized the error in the measurements made by the observers, thus leading to the high ICC. To further standardize this evaluation, software to determine these lines automatically is essential. Regardless of the limitations, however, our study did show that 1050-nm SS-OCT provides a unique opportunity to study macular choroidal thickness in three dimensions. Furthermore, our results have confirmed the asymmetric nature of macular choroidal thickness. Further studies using pathologic eyes are, of course, necessary to establish the validity and usefulness of choroidal thickness maps obtained with SS-OCT at this longer wavelength.

References

1. Townsend KA, Wollstein G, Schuman JS. Clinical application of MRI in ophthalmology. *NMR Biomed.* 2008;21:997-1002.
2. Coleman DJ, Silverman RH, Chabi A, et al. High-resolution ultrasonic imaging of the posterior segment. *Ophthalmology.* 2004; 111:1344-1351.
3. Drexler W, Sattmann H, Hermann B, et al. Enhanced visualization of macular pathology with the use of ultrahigh-resolution optical coherence tomography. *Arch Ophthalmol.* 2003;121:695-706.
4. Ko TH, Fujimoto JG, Schuman JS, et al. Comparison of ultrahigh- and standard-resolution optical coherence tomography for imaging macular pathology. *Ophthalmology.* 2005;112:1922-1935.
5. Wojtkowski M, Bajraszewski T, Gorczynska I, et al. Ophthalmic imaging by spectral optical coherence tomography. *Am J Ophthalmol.* 2004;138:412-419.
6. Ikuno Y, Tano Y. Retinal and choroidal biometry in highly myopic eyes with spectral-domain optical coherence tomography. *Invest Ophthalmol Vis Sci.* 2009;50:3876-3880.
7. Ikuno Y, Jo Y, Hamasaki T, Tano Y. Ocular risk factors for choroidal neovascularization in pathologic myopia. *Invest Ophthalmol Vis Sci.* 2010;51:3721-3725.
8. van Velthoven ME, Faber DJ, Verbraak FD, van Leeuwen TG, de Smet MD. Recent developments in optical coherence tomography for imaging the retina. *Prog Retin Eye Res.* 2007;26:57-77.
9. Spaide RF, Koizumi H, Pozzoni MC. Enhanced depth imaging spectral-domain optical coherence tomography. *Am J Ophthalmol.* 2008;146:496-500.
10. Spaide RF. Enhanced depth imaging optical coherence tomography of retinal pigment epithelial detachment in age-related macular degeneration. *Am J Ophthalmol.* 2009;147:644-652.
11. Margolis R, Spaide RF. A pilot study of enhanced depth imaging optical coherence tomography of the choroid in normal eyes. *Am J Ophthalmol.* 2009;147:811-815.
12. Reibaldi M, Boscia F, Avitabile T, et al. Enhanced depth imaging optical coherence tomography of the choroid in idiopathic macular hole: a cross-sectional prospective study. *Am J Ophthalmol.* 2011;151:112-117.
13. Maruko I, Iida T, Sugano Y, et al. Subfoveal choroidal thickness after treatment of Vogt-Koyanagi-Harada disease. *Retina.* 2011;31:510-517.
14. Maruko I, Iida T, Sugano Y, Ojima A, Ogasawara M, Spaide RF. Subfoveal choroidal thickness after treatment of central serous chorioretinopathy. *Ophthalmology.* 2010;117:1792-1799.
15. Imamura Y, Iida T, Maruko I, Zweifel SA, Spaide RF. Enhanced depth imaging optical coherence tomography of the sclera in dome-shaped macula. *Am J Ophthalmol.* 2011;151:297-302.
16. Chung SE, Kang SW, Lee JH, Kim YT. Choroidal thickness in polypoidal choroidal vasculopathy and exudative age-related macular degeneration. *Ophthalmology.* 2011;118:840-845.
17. Koizumi H, Yamagishi T, Yamazaki T, Kawasaki R, Kinoshita S. Subfoveal choroidal thickness in typical age-related macular degeneration and polypoidal choroidal vasculopathy. *Graefes Arch Clin Exp Ophthalmol.* In press.
18. Fong AH, Li KK, Wong D. Choroidal evaluation using enhanced depth imaging spectral-domain optical coherence tomography in Vogt-Koyanagi-Harada disease. *Retina.* 2011;31:502-509.
19. Vance SK, Imamura Y, Freund KB. The effects of sildenafil citrate on choroidal thickness as determined by enhanced depth imaging optical coherence tomography. *Retina.* 2011;31:332-335.
20. Fujiwara T, Imamura Y, Margolis R, Slakter JS, Spaide RF. Enhanced depth imaging optical coherence tomography of the choroid in highly myopic eyes. *Am J Ophthalmol.* 2009;148:445-450.
21. Yeoh J, Rahman W, Chen F, et al. Choroidal imaging in inherited retinal disease using the technique of enhanced depth imaging optical coherence tomography. *Graefes Arch Clin Exp Ophthalmol.* 2010;248:1719-1728.
22. Mwanza JC, Hochberg JT, Banitt MR, Feuer WJ, Budenz DL. Lack of association between glaucoma and macular choroidal thickness measured with enhanced depth imaging optical coherence tomography. *Invest Ophthalmol Vis Sci.* 2011;52:3430-3435.
23. Rahman W, Chen FK, Yeoh J, Patel P, Tufail A, Da Cruz L. Repeatability of manual subfoveal choroidal thickness measurements in healthy subjects using the technique of enhanced depth imaging optical coherence tomography. *Invest Ophthalmol Vis Sci.* 2011;52: 2267-2271.
24. McCourt EA, Cadena BC, Barnett CJ, Ciardella AP, Mandava N, Kahook MY. Measurement of subfoveal choroidal thickness using spectral domain optical coherence tomography. *Ophthalmic Surg Lasers Imaging.* 2010;41(suppl):S28-S33.
25. Imamura Y, Fujiwara T, Margolis R, Spaide RF. Enhanced depth imaging optical coherence tomography of the choroid in central serous chorioretinopathy. *Retina.* 2009;29:1469-1473.
26. Maruko I, Iida T, Sugano Y, Saito M, Sekiryu T. Subfoveal retinal and choroidal thickness after verteporfin photodynamic therapy for polypoidal choroidal vasculopathy. *Am J Ophthalmol.* 2011; 151:594-603.
27. Yasuno Y, Okamoto F, Kawana K, Yatagai T, Oshika T. Investigation of multifocal choroiditis with panuveitis by three-dimensional high-penetration optical coherence tomography. *J Biophotonics.* 2009;2:435-441.
28. Esmaeelpour M, Povazay B, Hermann B, et al. Three-dimensional 1060-nm OCT: choroidal thickness maps in normal subjects and improved posterior segment visualization in cataract patients. *Invest Ophthalmol Vis Sci.* 2010;51:5260-5266.
29. Povazay B, Bizheva K, Hermann B, et al. Enhanced visualization of choroidal vessels using ultrahigh resolution ophthalmic OCT at 1050 nm. *Opt Express.* 2003;11:1980-1986.
30. Huber R, Adler DC, Srinivasan VJ, Fujimoto JG. Fourier domain mode locking at 1050 nm for ultra-high-speed optical coherence tomography of the human retina at 236,000 axial scans per second. *Opt Lett.* 2007;32:2049-2051.
31. Ikuno Y, Kawaguchi K, Nouchi T, Yasuno Y. Choroidal thickness in healthy Japanese subjects. *Invest Ophthalmol Vis Sci.* 2010;51: 2173-2176.
32. Lee EC, de Boer JF, Mujat M, Lim H, Yun SH. In vivo optical frequency domain imaging of human retina and choroid. *Opt Express.* 2006;14:4403-4411.